Bundle Adjustment with Additional Constraints Applied to Imagery of the Dunhuang Wall Paintings

Yongjun Zhang Kun Hu Rongyong Huang

School of Remote Sensing and Information Engineering, Wuhan University,

No. 129 Luoyu Road, Wuhan, 430079, P.R. China (zhangyj@whu.edu.cn)

Abstract:

In the digital conservation of the Dunhuang wall painting, bundle adjustment is a critical step in precise orthoimage generation. The error propagation of the adjustment model is accelerated because the near-planar photographic object intensifies correlation of the exterior orientation parameters and the less than 60 percent forward overlap of adjacent images weakens the geometric connection of the network. According to the photographic structure adopted in this paper, strong correlation of the exterior orientation parameters can be verified theoretically. In practice, the additional constraints of near-planarity and exterior orientation parameters are combined with bundle adjustment to control the error propagation. The positive effects of the additional constraints are verified by experiments, which show that the introduction of weighted observation equations into bundle adjustment contributes a great deal to the theoretical and actual accuracies of the unknowns as well as the stability of the adjustment model.

Keywords: Dunhuang wall painting imagery; bundle adjustment; additional constraints; correlation analysis; accuracy

1. INTRODUCTION

As an important cultural heritage of China, the Dunhuang wall painting is of great value for both historical investigation and arts appreciation. Under the construction of “Digital Dunhuang,” it’s an urgent task to reproduce the painting as a high precision orthoimage with close-range photogrammetric techniques, which involves image matching, bundle adjustment, ortho-rectification, color correction, etc. (Zhang et al., 2011). Bundle adjustment is performed to obtain the precise exterior orientation parameters and the coordinates of the object points, and is widely used for the digital surface model generation of cultural heritages (El-Hakim et al., 2004; Arias et al., 2005). Since the painting lies on a near-planar wall surface and the forward overlap between adjacent images is smaller than 60 percent, the correlation of the exterior orientation parameters and the condition number of the normal matrix increase significantly, with the accuracy and reliability of the unknowns decreasing therefrom. Hence, the algorithm design of the bundle adjustment process needs to improve.

To describe the influence of the photographic structure on the adjustment model, it’s an efficient way to analysis the correlation of parameters. The redundancy and relativity of the observations were analyzed based on derivative collinearity equations in generalized point photogrammetry, so were the minimal observations and accuracy distribution of the space resection (Zhang et al., 2005). Four relations among nine orientation parameters of two cameras were found to be in direct relative orientation, and a kind of “Five-Point” algorithm that was suitable for numerical implementation and which corresponded to the inherent complexity of the problem was proposed (Nistér, 2004; Stewénius et al., 2006). Regarding the correlation problem of unknown parameters in bundle adjustment, experiments and statistical charts were adopted to analyze the variation of standard error and the correlation coefficient of the parameters that related to the photographic structure (Jacobsen, 1999; Lichti et al., 2010; Mass,

2009). Theoretical analysis of reliability and sensibility is also beneficial for the adjustment model selection and triangular network design. Measures can be taken to remove the correlation of the parameters and the singularity of the normal matrix, thus improving the quality of the solutions (Triggs et al., 2000). With regard to circular imaging particularly, Heikkinen (2004) took advantage of the circularity and coplanarity condition of projection centers to parameterize the equations in bundle adjustment. The circular image block method in real measuring tasks was evaluated in terms of accuracy and robustness.

Relative control is a certain known geometric relationship among the unknown points in photogrammetric processing, which can enhance the intensity for photogrammetric work and for inspection of the accuracy and reliability for photogrammetry (Feng, 2001). In the field of computer vision as well, geometric relationships are commonly embodied in the motion of camera (Hernández et al., 2007), the relative position of stereo cameras (Malm et al., 2001), and the characteristic of object space, which contribute to camera self-calibration and 3D modeling. Different types of geometric constraints can be applied in case of redundancy in bundle adjustment, which include topology constraints (e.g., object point constraint, object line constraint, and coplanarity) and object constraints (e.g., parallelism, perpendicularity, and symmetry) (van den Heuvel, 1998). Least-squares estimates of the 3D points, camera position orientation are recovered precisely by exploiting planes, alignments, symmetries, orthogonalities, and other forms of geometrical regularity (Grossmann et al., 2005). The integration of parallelism constraint on planes and line-photogrammetric bundle adjustment results in a valid polyhedral description of the object, which offers the advantage of processing a model without real control points on the condition that the exterior orientation parameters are approximately known (Hrabácek et al., 2000). When an object is rotating around a single axis with varying camera internal parameters, the constant rotation angle and circular motion are employed to refine the camera parameters from coarse to fine (Cao et al., 2006).

Based on the photographic structure of the Dunhuang wall painting, this paper analyzes the correlation of the exterior orientation parameters, presents a novel bundle adjustment model with additional constraints of near-planarity and exterior orientation parameters, and assesses the effect of weighted observation equations on the theoretical and actual accuracies of the unknowns. This paper is organized as follows: In Section 2, the correlation coefficients of the exterior orientation parameters are calculated on an assumption of the geometric relationship. Section 3 presents several methods that introduce the planarity constraints into the adjustment model; and the design of the combined bundle adjustment is illustrated in detail. Experiments are carried out in Section 4 to measure the effect of the weighted observation equations in bundle adjustment. Finally, Section 5 presents our conclusions.

2. PHOTOGRAPHIC STRUCTURE AND CORRELATION ANALYSIS

2.1 Photographic structure

There were more than 20,000 images of wall paintings captured in about 100 caves a few years ago without the purpose of photogrammetric processing at the time of data acquisition. However, these data are used for bundle adjustment and orthoimage generation during our work. The design and layout of the photographic structure is shown in Fig. 1: The test painting lies on a near-planar wall surface. A pre-calibrated digital camera is fixed on an orbital platform that is near-parallel to the painting. The images are captured along regular strips, with the forward overlap and sidelap between adjacent images maintained at 50 percent. The principal optical axes of the images are parallel with each other and perpendicular to the painting; and the origin of the object space coordinate system is set at the lower left corner of the painting, with the X-axis parallel to the track, the Y-axis pointing to the zenith, and the Z-axis perpendicular to the painting.

According to the photographic structure of the painting, the geometric relationship can be simplified as imaging

on a plane to near-planar surface under the condition of normal case photography (i.e., the photographic distance and scale remain approximately constant). Owing to the small overlap between images, the geometric connection is weak and the adjustment model is unstable. The correlation problem among the parameters is intensified because of the near-planar photographic object, which is verified in Section 2.2 theoretically. Hence, additional constraints should be taken into consideration for a better solution of bundle adjustment.

Fig. 1 Photographic structure of the painting (Zhang et al., 2011)

2.2 Correlation analysis of exterior orientation parameters

Based on the perspective projection between a three-dimensional space and a plane (Mikhail et al., 2001), the relationship between each object point on the painting and the corresponding image point can be described as follow:

$$\begin{bmatrix} X-X_s \\ Y-Y_s \\ Z-Z_s \end{bmatrix} = \lambda \mathbf{R} \begin{bmatrix} x \\ y \\ -f \end{bmatrix} = \lambda \begin{bmatrix} r_{11} & r_{12} & r_{13} \\ r_{21} & r_{22} & r_{23} \\ r_{31} & r_{32} & r_{33} \end{bmatrix} \begin{bmatrix} x \\ y \\ -f \end{bmatrix} \tag{1}$$

where (X, Y, Z) and (X_s, Y_s, Z_s) are the coordinates of the object point and the projection center in the object space coordinate system, respectively, $(x, y, -f)$ the coordinates of the corresponding image point in the image space coordinate system, λ the scale factor, $\mathbf{R}$ the rotation matrix containing the rotation parameters $r_{11}, r_{12}, \ldots, r_{33}$.

The standard approach to construct $\mathbf{R}$ is by using three sequential rotations: φ about the Y-axis, ω about the once-rotated X-axis, and κ about the twice-rotated Z-axis (Mikhail et al., 2001). The rotation matrix $\mathbf{R}$ then can be expressed as follows:

$$\mathbf{R} = \mathbf{R}_\varphi \mathbf{R}_\omega \mathbf{R}_\kappa = \begin{bmatrix} \cos\varphi\cos\kappa - \sin\varphi\sin\omega\sin\kappa & -\cos\varphi\sin\kappa - \sin\varphi\sin\omega\cos\kappa & -\sin\varphi\cos\omega \\ \cos\omega\sin\kappa & \cos\omega\cos\kappa & -\sin\omega \\ \sin\varphi\cos\kappa + \cos\varphi\sin\omega\sin\kappa & -\sin\varphi\sin\kappa + \cos\varphi\sin\omega\cos\kappa & \cos\varphi\cos\omega \end{bmatrix} \tag{2}$$

The rotation angles, including φ, ω, and κ, are almost equal to zero under the approximate condition of

normal case photography. Linear terms are then selected to simplify the expression.

$$\begin{bmatrix} X - X_s \\ Y - Y_s \\ Z - Z_s \end{bmatrix} = \lambda \begin{bmatrix} 1 & -\kappa & -\varphi \\ \kappa & 1 & -\omega \\ \varphi & \omega & 1 \end{bmatrix} \begin{bmatrix} x \\ y \\ -f \end{bmatrix} \tag{3}$$

Regarding the geometric relationship of the photographic structure, the scale factor λ can be considered as an invariant. There are three equations determined by each pair of conjugate points. These equations are expanded and simplified as follows:

$$\begin{cases} X_s = X - \lambda(x - y\kappa + f\varphi) \\ Y_s = Y - \lambda(x\kappa + y + f\omega) \\ Z_s = Z - \lambda(x\varphi + y\omega - f) \end{cases} \tag{4}$$

i.e.:

$$\begin{bmatrix} 1 & 0 & 0 & \lambda f & 0 & -\lambda y \\ 0 & 1 & 0 & 0 & \lambda f & \lambda x \\ 0 & 0 & 1 & \lambda x & \lambda y & 0 \end{bmatrix} \begin{bmatrix} X_s \\ Y_s \\ Z_s \\ \varphi \\ \omega \\ \kappa \end{bmatrix} + \begin{bmatrix} 1 & 0 & 0 \\ 0 & 1 & 0 \\ 0 & 0 & 1 \end{bmatrix} \begin{bmatrix} X \\ Y \\ Z \end{bmatrix} = \begin{bmatrix} -\lambda x \\ -\lambda y \\ \lambda f \end{bmatrix} \tag{5}$$

In order to analyze the correlation of the exterior orientation parameters, it's an efficient way to calculate the correlation coefficient between each two columns of the coefficient matrix of Eq. (5). The correlation coefficient may be viewed as a normalized version of the covariance function, which can be treated as a statistical indicator to reflect the closeness of the relationships between variables (Bertsekas et al., 2008). If the correlation coefficient between two columns is close to 1, the probability that the two columns meet with a linear relationship is close to 1.

First, taking the correlation between the linear element X_s and the angular element φ into consideration, the correlation coefficient between the corresponding two columns of Eq. (5) is:

$$\rho(X_s,\varphi)=\frac{\sum \lambda f}{\sqrt{\sum 1\sum \lambda^2(f^2+x^2)}}=\frac{\lambda nf}{\sqrt{n\lambda^2\sum(f^2+x^2)}}=\frac{1}{\sqrt{1+\frac{1}{n}\sum(\frac{x}{f})^2}}\approx 1 \tag{6}$$

Similarly, the correlation coefficient between two columns related to X_s and ω is close to 0, while the one related to X_s and κ is calculated as follow:

$$\rho(X_s,\kappa)=\frac{\sum -\lambda y}{\sqrt{n\sum \lambda^2(x^2+y^2)}}=\frac{-\sum y}{\sqrt{n\sum(x^2+y^2)}} \tag{7}$$

If the image points are widely distributed within the image format, a relationship of the coordinates of the image points exists as follow:

$$\sum y << \sqrt{n\sum(x^2+y^2)} \tag{8}$$

Based on this, the correlation coefficient related to X_s and κ is close to 0.

If a linear relationship exists between two columns of the coefficient matrix of the linear equations, the linear relationship between the corresponding two unknowns can be derived. Therefore, when imaging on a plane to near-planar surface under the condition of normal case photography, the linear element X_s is highly correlated with the angular element φ, rather than with other angular elements.

Similarly, the linear element Y_s is highly correlated with the angular element ω rather than with other angular elements. Within the restrictions of the photographic structure, when using bundle adjustment based on the collinearity equations (refer to Eq. (11)), strong correlations exist between the columns of the normal matrix corresponding to X_s and φ and Y_s and ω of each image, respectively. Both the strong correlation of the exterior orientation parameters and the small overlap between the images intensifies the singularity of the normal equation, which seriously decreases the accuracy of the unknowns.

3. DESIGN OF BUNDLE ADJUSTMENT WITH ADDITIONAL CONSTRAINTS

3.1 Methods of introducing planarity constraints

One logical way of dealing with the strong correlation problem is to select or merge certain parameters in bundle adjustment, such as the additional parameters in camera calibration (Remondino et al., 2006), and the exterior orientation parameters of linear array scanner images (Gruen et al, 2005). Another approach is to take advantages of the position characteristic of the projection centers, for instance, the linear element Z_s is treated as a pseudo observation because the projection centers of all the images are nearly coplanar (Zhang et al., 2011). Moreover, the geometric constraints of the object space also can be taken into consideration. In this photographic structure, it is convenient to take advantage of the planarity constraints of the painting to strengthen the geometric connection and control the error propagation of the adjustment model.

For a plane in any direction, the relationship of the object points can be expressed by the general form of a plane equation as follow:

$$aX + bY + cZ + d = 0 \qquad (a^2 + b^2 + c^2 = 1) \tag{9}$$

where (X, Y, Z) are the coordinates of the object point on the painting in the object space coordinate system, a, b, c and d of the plane equation parameters.

There are two methods for introducing Eq. (9) into the adjustment model. The former is to introduce the planarity constraints as a true value in order to attain “adjustment by elements with constraints” (Fan, 2005); while the latter would introduce the planarity constraints as weighted observations in order to accomplish “adjustment by elements with pseudo observations” (Fan, 2005).

Since the painting does not lie on a strict plane, the second method is more suitable for the photographic

structure. Then, Eq. (9) can be converted into error equations and linearized using the Taylor series expansion as follows:

$$\begin{aligned} V_{plane} &= a^0\Delta_X + b^0\Delta_Y + c^0\Delta_Z + X\Delta_a + Y\Delta_b + Z\Delta_c + \Delta_d + (aX + bY + cZ + d) \\ V_{res} &= 2a\Delta_a + 2b\Delta_b + 2c\Delta_c + (a^2 + b^2 + c^2 - 1) \end{aligned} \tag{10}$$

where V_{plane} and V_{res} are the correction terms of the observations; Δ_X, Δ_Y, and Δ_Z the correction terms of X, Y, and Z; $\Delta_a, \Delta_b, \Delta_c$, and Δ_d the correction terms of a, b, c, and d; and a^0, b^0, and c^0 the first-order partial derivatives of planarity constraints determined by X, Y, and Z, respectively.

The unknowns of the error equations include both the correction terms of the coordinates of the object points and the plane equation parameters.

3.2 Adjustment with additional constraints

The additional constraints combined in the bundle adjustment in this paper include the constraints of the exterior orientation parameters that are highly correlated in Section 2.2 and the constraints of near-planarity according to the second method in Section 3.1. In bundle adjustment, all the coordinates of the object points and the corresponding image points fit with the collinearity equations. The basic model is (Mikhail et al., 2001):

$$\begin{cases} x - x_0 = -f\dfrac{r_{11}(X - X_s) + r_{12}(Y - Y_s) + r_{13}(Z - Z_s)}{r_{31}(X - X_s) + r_{32}(Y - Y_s) + r_{33}(Z - Z_s)} \\ y - y_0 = -f\dfrac{r_{21}(X - X_s) + r_{22}(Y - Y_s) + r_{23}(Z - Z_s)}{r_{31}(X - X_s) + r_{32}(Y - Y_s) + r_{33}(Z - Z_s)} \end{cases} \tag{11}$$

where the significance of all the parameters are the same as those in Eq. (1).

Considered the strong correlations between X_s and φ, Y_s and ω of each image, respectively, φ and ω are treated as weighted observations. Considered the geometric constraints of the painting, Eq. (10) is also treated as the weighted observation equation in the adjustment model. After linearization, the observation equations

of the combined adjustment model have the following form:

$$\begin{cases} \mathbf{V}_{x,y} = \mathbf{AT} + \mathbf{BM} & -\mathbf{L}_1 & \mathbf{P}_1 \\ \mathbf{V}_{plane} = & \mathbf{CM} + \mathbf{DN} - \mathbf{L}_2 & \mathbf{P}_2 \\ \mathbf{V}_{res} = & \mathbf{FN} - \mathbf{L}_3 & \mathbf{P}_3 \\ \mathbf{V}_{\varphi,\omega} = \mathbf{T}_{\varphi,\omega} & & \mathbf{P}_4 \end{cases} \tag{12}$$

where $\mathbf{V}_{x,y}$ and $\mathbf{V}_{\varphi,\omega}$ the correction vectors of the observations; $\mathbf{M}=[\Delta X\ \Delta Y\ \Delta Z]^T$ and $\mathbf{T}=[\Delta X_s\ \Delta Y_s\ \Delta Z_s\ \Delta\varphi\ \Delta\omega\ \Delta\kappa]^T$ the correction vectors of the coordinates of the object points and exterior orientation parameters, respectively; $\mathbf{T}_{\varphi,\omega}$ the correction vector of φ and ω; $\mathbf{N}=(\Delta a\ \Delta b\ \Delta c\ \Delta d)^T$ the correction vector of plane equation parameters; $\mathbf{A},\mathbf{B},\mathbf{C},\mathbf{D},\mathbf{F}$ the designed matrix of the correction vectors above; $\mathbf{L}_1,\mathbf{L}_2$, and $\mathbf{L}_3$ the constant items calculated by the approximate values of the unknowns; and $\mathbf{P}_1,\mathbf{P}_2,\mathbf{P}_3$, and $\mathbf{P}_4$ the weight matrices of the observation equations.

The appropriate weight matrix of the error equations plays an important role in improving the accuracy of the unknowns and speeding up the convergence rates. The initial weight matrix of the collinearity equations is set to be the unit matrix. The weight of equation $a^2+b^2+c^2=1$ is set to be a large value diagonal matrix because of the absolute constraint relations. The initial weight matrices of the pseudo observation equations should consist with their a priori accuracies against the unit weight variance (Zhang et al., 2011), in which the coplanar state of the painting and the correlation coefficient of the exterior orientation parameters should be considered.

The normal equation is described as follow:

$$\begin{bmatrix} \mathbf{A}^{\mathbf{T}}\mathbf{P}_1\mathbf{A}+\mathbf{P}_4 & \mathbf{A}^{\mathbf{T}}\mathbf{P}_1\mathbf{B} & \mathbf{0} \\ \mathbf{B}^{\mathbf{T}}\mathbf{P}_1\mathbf{A} & \mathbf{B}^{\mathbf{T}}\mathbf{P}_1\mathbf{B}+\mathbf{C}^{\mathbf{T}}\mathbf{P}_2\mathbf{C} & \mathbf{C}^{\mathbf{T}}\mathbf{P}_2\mathbf{D} \\ \mathbf{0} & \mathbf{D}^{\mathbf{T}}\mathbf{P}_2\mathbf{C} & \mathbf{D}^{\mathbf{T}}\mathbf{P}_2\mathbf{D}+\mathbf{F}^{\mathbf{T}}\mathbf{P}_3\mathbf{F} \end{bmatrix} \begin{bmatrix} \mathbf{T} \\ \mathbf{M} \\ \mathbf{N} \end{bmatrix} = \begin{bmatrix} \mathbf{A}^{\mathbf{T}}\mathbf{P}_1\mathbf{L}_1 \\ \mathbf{B}^{\mathbf{T}}\mathbf{P}_1\mathbf{L}_1+\mathbf{C}^{\mathbf{T}}\mathbf{P}_2\mathbf{L}_2 \\ \mathbf{D}^{\mathbf{T}}\mathbf{P}_2\mathbf{L}_2+\mathbf{F}^{\mathbf{T}}\mathbf{P}_3\mathbf{L}_3 \end{bmatrix} \tag{13}$$

The exterior orientation parameters of all the images, the coordinates of all the object points, and the four plane equation parameters need to be calculated meanwhile in the combined bundle adjustment model through total

iteration.

If control points are considered in this adjustment model, the error equations determined by the control points need to be combined with Eq. (12). The linearized form is:

$$\mathbf{V}_{x_G,y_G} = \mathbf{GT} - \mathbf{L}_5 \quad \mathbf{P}_5 \tag{14}$$

where $\mathbf{V}_{x_G,y_G}$ is the correction vector of the observations, $\mathbf{G}$ the designed matrix of the correction vector $\mathbf{T}$; $\mathbf{L}_5$ the constant item; and $\mathbf{P}_5$ the weight matrix consistent with the control level.

To verify the effect of the additional constraints on the bundle adjustment model, it is necessary to assess the theoretical and actual accuracies of the unknowns. Actual accuracy is calculated by the root mean square (RMS) error using the check points, while theoretical accuracy calculates the inverse matrix of the normal matrix and the extract diagonal elements. The expression of theoretical accuracy is (Fan, 2005):

$$\sigma_i = \sigma_0 \sqrt{\mathbf{Q}_{ii}} \tag{15}$$

4. EXPERIMENTS AND RESULTS

4.1 Data sources

According to the photographic structure of the Dunhuang wall painting referenced in Section 2.1, a test painting is used for experiments in this paper. The length and width of the painting are about 4 m and 2.5 m, respectively, with a 0.13 m deflection at the top of the painting. There are 734 images captured along 16 strips at a distance of about 0.5 m with 20,830 conjugate points matched. The image format, pixel size, and principal distance of the camera are 35.9424 mm×23.9616 mm, 0.0064 mm, and 53 mm, respectively. The ground sample distance (GSD) is calculated as 0.065 mm. There are 56 widely distributed object points measured by an electronic total station with a 1 mm + 1 ppm nominal accuracy of the distance measurement. Therefore, the plane and elevation accuracies of these points are

about 1.0 mm and 2.0 mm, respectively.

Given an orientation standard, the initial values of the exterior orientation parameters in bundle adjustment are calculated by image matching and relative orientation of adjacent images. The initial values of the coordinates of object points are calculated through space intersection from multiple images. According to the photographic structure of the painting illustrated in Section 2.1, the principal optical axes of the images are parallel with each other and perpendicular to the painting, and the images are captured at a distance of about 0.5 m, so the initial values of the plane parameters a, b, c, and d are set at 0.0, 0.0, 1.0 and 50.0, respectively. The new approximations of the parameters are determined by a plus of the approximations with adjusted corrections in the last time during iterations.

4.2 Experiment on correlation of exterior orientation parameters

To verify the correlation problem of the exterior orientation parameters for the photographic structure, the correlation coefficient between the two columns of the error equations corresponding to a linear element and an angular element are calculated.

Table 1 Correlation coefficient of exterior orientation parameters

As shown in Table 1, the terms “Max”, “Min” and “Mean” stand for the maximum value, the minimum value and the arithmetic average value of the corresponding items, respectively. The correlation coefficients between the columns corresponding to X_s and φ, Y_s and ω, respectively, are close to 1, while the others are relatively small. The results verify the theoretical derivation in Section 2.2, namely, strong correlations exist between X_s and φ and Y_s and ω, respectively. Hence, it is reasonable to treat φ and ω as weighted observations in bundle adjustment, by which to decrease the correlation and improve the geometric configuration of the adjustment model.

4.3 Experiment on Bundle Adjustment without Control Points

Since it is an efficient way to reveal the error propagation, the minimally constrained block adjustment is employed in this section, with the exterior orientation parameters of the first image and the baseline with the second image on the first strip fixed. The weights of the constraints of near-planarity and exterior orientation parameters are set at 0.001 and 20, respectively, as the method illustrated in Section 2.2. Then, comparisons of the theoretical accuracy of the unknowns are made based on whether or not the weighted observation equations are introduced.

Model I is bundle adjustment without these additional constraints, while Model II is bundle adjustment with them as the virtual observations. The unit weight RMS errors of Model I and Model II are 0.006286 and 0.007504, respectively, the condition numbers of the corresponding normal matrices are 1.5733*10^26 and 2.0302*10^24, respectively, and the iteration times are 14 and 7, respectively. Compared with the solutions of Model I, the unit weight RMS error of Model II increases to 1.2 pixels because of the quasi-planarity constraints; whereas, the condition number is reduced by about 500 times, and the iteration times are reduced by 50 percent. The results show that the additional constraints can not only speed up the convergence rate, but also improve the geometric configuration and stability of the adjustment model.

Details regarding the theoretical accuracy statistics of the exterior orientation parameters and the coordinates of the object points are shown in Table 2. As can be seen, the solutions of Model II are better than those of Model I, as well as the theoretical accuracy of the exterior orientation parameters. In spite of a small increase in the minimum value, the theoretical accuracy of the object points in Model II is also improved and consistent with the GSD and the accuracy of image matching, which is usually 0.3 pixels.

Table 2 Theoretical accuracy of unknowns in Model I and Model II (without control points)

To illustrate the rapid decrease problem of the solutions in Model I, the 43 largest values of the theoretical

accuracy of the object points are selected, which are between 0.13477 and 1.12597 in the X direction, 0.09840 and 1.32630 in the Y direction, and 0.35386 and 4.81030 in the Z direction. This problem is caused by the lack of geometric connection in a certain part of the adjustment model. However, this problem does not occur in Model II. The results show that the additional constraints can strengthen the geometric connection and the stability of the adjustment model, as well as improving the theoretical accuracy of the unknowns effectively.

Furthermore, the theoretical accuracy distribution of the object points needs to be described. Taking the X and Z direction, for example, comparisons of the theoretical accuracy of the object points are made based on whether or not the weighted observation equations are introduced. Two-dimensional interpolation of the cubic spline surfaces is employed to describe the distribution, and the position of the first fixed image is marked out by a vertical red line. The theoretical accuracy distribution of the object points in Model I and Model II are shown in Fig. 2(a) to 2(d). For convenience of comparison, the 43 singular values are not considered.

Fig. 2. Theoretical accuracy distribution of object points: (a) and (b), (c) and (d) are the RMS errors of Model I and Model II in the X and Z direction, respectively; (e) and (f), (g) and (h) are the RMS errors of Model III and Model IV in the X and Z direction, respectively.

As can be seen, a growing trend of the theoretical accuracy is from the beginning position of the first fixed image that meets with the law of error propagation (i.e., the farther an object point is from the control condition, the less influence the control function exerts and the less accurate it is). The theoretical accuracy of the object points distributes uniformly in the interior area of the painting but grows worse rapidly in the edge area because the images near the edge are lack of geometric connection. There are several protruding portions because the corresponding image points are badly matched. When compared to the solutions of Model I, the plane accuracy of the object points in Model II is improved slightly and the elevation accuracy is noticeably better. Owing to the additional constraints, the error propagation of Model II in the Z direction is controlled effectively and the solutions distribute more homogeneously. Hence, it is useful to introduce these constraints into the adjustment model under the condition of

bundle adjustment without control points.

4.4 Experiment on Bundle Adjustment with Control Points

Widely distributed control points are normally laid out and participate in bundle adjustment in order to take control of error propagation. The effect of the additional constraints needs to be investigated as well. Fifteen of the 56 object points measured by a total station (Section 4.1) are regarded as control points, while the others are regarded as check points. The weights of the constraints of near-planarity and exterior orientation parameters are the same as those in Section 4.3. Comparisons of the theoretical accuracy of the unknowns are made based on whether or not the weighted observation equations are introduced.

Model III is bundle adjustment without these additional constraints, while Model IV is bundle adjustment with them as virtual observations. The unit weight RMS errors of Model III and Model IV are 0.006495 and 0.006901, respectively, the condition numbers of the normal matrix are 8.9732*10^21 and 1.3667*10^20, respectively, and the iteration times are 11 and 6, respectively. When compared to the solutions in Section 4.3, the unit weight RMS error and condition number are much better if the control points are considered in the adjustment model. Moreover, the solutions of Model IV are better than those of Model III. The results show that the control points can also speed up the convergence rate and improve the geometric configuration and stability of the adjustment model, while the additional constraints make the solutions even better. Details of the theoretical accuracy statistics of the exterior orientation parameters and the coordinates of the object points are shown in Table 3.

Table 3 Theoretical accuracy of unknowns in Model III and Model IV (with control points)

Owing to the widely distributed control points, the theoretical accuracy of the exterior orientation parameters and the coordinates of the object points in Table 3 are improved when compared to the results in Table 2. Also, the solutions of Model IV are better than those of Model III if the weighted observation equations are introduced into the

adjustment model. The results show that the additional constraints are significant also in bundle adjustment regardless of the positive effect of the control points.

Similarly, if the control points are taken into consideration, comparisons of the theoretical accuracy of the unknowns in the X and Z direction are made based on whether or not the weighted observation equations are introduced. The theoretical accuracy distribution is shown in Fig. 2(e) to 2(h). The singular valves are not considered likewise.

By comparisons of Fig. 2(a) to 2(d) and Fig. 2(e) to 2(h), improvement of the theoretical accuracy of the object points by the control points and the weighted observation equations are verified. The control points improve both the plane accuracy and elevation accuracy, while the additional constraints have greater effects on elevation accuracy than on plane accuracy, reaching a higher and more homogeneously distributed accuracy of the unknowns in spite of the control points. The combination of additional constraints and control points in bundle adjustment reach the best solutions in all the foregoing experiments.

In order to verify the improvement of the actual accuracy of the unknowns related to the weighted observation equations, 41 check points are selected in Model III and Model IV. Comparisons of actual accuracy of the unknowns are made based on whether or not the weighted observation equations are introduced. The statistics are shown in Table 4.

Table 4 Actual accuracy of check points in Model III and Model IV (with control points)

The statistical regularities of actual accuracy shown in Table 4 are similar to those in Table 3, which illustrates that the additional constraints can not only improve the theoretical accuracy but also can improve the actual accuracy of the unknowns. However, the actual accuracy is worse than the corresponding theoretical accuracy because the theoretical accuracy of the unknowns is affected only by the quality of the observations and the geometric

configuration of the adjustment model, while the actual accuracy of the unknowns is affected by the quality and distribution of the control points and check points as well. As illustrated in Section 4.1, the plane and elevation accuracies of these points are 1.0 mm and 2.0 mm, respectively; therefore, it is reasonable to state that the actual accuracy is consistent with the control level.

4.5 Experiment on Weights of Additional Constraints

The weights of additional constraints of near-planarity and exterior orientation parameters are important to the stability of the adjustment model and the reliability of the solutions. For analysis, bundle adjustment without control points is employed in this paper, and the date sources are the same as those in Section 4.3. The weights of exterior orientation parameter constraints and near-planarity constraints are called Weight I and Weight II, respectively. Weight I is set at 1.0, 10.0 and 100.0, and Weight II is set at 0.0001, 0.001 and 0.01, respectively. Then nine tests are made and the unit weight RMS errors, condition numbers, iteration times, and mean value of theoretical accuracies in X, Y and Z directions are shown in Table 5,

Table 5 Solutions under different weights of constraints (without control points)

As can be seen, the unit weight RMS error increases slightly with the increase of Weight I and Weight II. When Weight I is kept constant, the condition number, iteration times and theoretical accuracies of Test II, Test V and Test VIII are better than the others if Weight II is set at 0.001. The theoretical accuracies in X, Y and Z directions are stable with the differences less than 0.005 mm. It’s important to set weight II consist with the coplanar state of the painting. If the near-planarity constraint is too weak, the convergence rate is slow down as well. On the contrary, if it’s set much larger beyond the actual conditions, the condition number increases significantly, which shows that the configuration of the adjustment model is unstable than the others. When Weight II is kept constant, the condition number and theoretical accuracies are getting better with the increase of Weight I, while the convergence rate is

getting slower. The exterior orientation parameters are strongly correlated as illustrated in Section 2.2 and 4.2. Hence, it's an efficient way to improve the theoretical accuracy of the results by giving Weight I a big value, particularly in the Z direction. The selection of the weights of constraints of near-planarity and exterior orientation parameters should be based on an overall consideration of the condition number, the theoretical accuracies and the iteration times.

5. CONCLUSIONS

Considered the photographic structure of the Dunhuang wall painting, the object is nearly flat and the forward overlap between adjacent images is about 50 percent, which lead to the configuration defects in the network. In order to resolve this problem, strong correlation of the exterior orientation parameters is derived theoretically. A novel combined bundle adjustment model with additional constraints is presented in this paper. The exterior orientation parameter constraints are used to decrease the correlation problem and improve the geometric configuration of the adjustment model, while the near-planarity constraints are used to strengthen the geometric connection and control error propagation in the adjustment model. The experiments show that the weighted observation equations play an important role in improving the theoretical and actual accuracies of the unknowns, as well as the stability of the adjustment model.

In practice, specifically dealing with the Dunhuang wall painting imagery in this paper, the additional constraints of near-planarity and the exterior orientation parameters are combined with the bundle adjustment to control the error propagation. The study can also be extended to other close-range photogrammetric applications which possess a similar geometric structure or the adjustment network is not strong enough. Furthermore, the strong correlation of the exterior orientation parameters can also be eliminated by merging the linear correlated components of the parameters

together during bundle adjustment. It awaits further studies on the accuracy improvement of the unknowns and comparison with the approach proposed in this paper.

ACKNOWLEDGEMENT

This work is supported by the National Natural Science Foundation of China with Project No. 41171292 and,41071233 the National Basic Research Program of China with Project No. 2012CB719904, and the National Key Technology Research and Development Program with Project No. 2011BAH12B05. We are very grateful also for the comments and contributions of anonymous reviewers and members of the editorial team.

REFERENCES

Arias, P., Herráez, J., Lorenzo, H., Ordóñez, C., 2005. Control of structural problems in cultural heritage monuments using close-range photogrammetry and computer methods. Computers and Structures 83 (21-22), 1754-1766.

Bertsekas, D. P., Tsitsiklis, J. N., 2008. Introduction to Probability, second ed. Athena Scientific, Belmont, MA.

Cao, X. C., Xiao, J. J., Foroosh, H., Shah, M., 2006. Self-calibration from turn-table sequences in presence of zoom and focus. Computer Vision and Image Understanding 102 (3), 227-237.

El-Hakim, S. F., Beraldin, J. -A., Picard, M., Godin, G., 2004. Detailed 3D reconstruction of large-scale heritage sites with integrated techniques. IEEE Computer Graphics and Applications 24 (3), 21-29.

Fan, H., 2005. Theory of errors and least squares adjustment. Royal Institute of Technology, Division of Geodesy, Stockholm, Sweden.

Feng, W. H., 2001. Control work in close range photogrammetry. Geo-spatial Information Science 4 (4), 66-72.

Grossmann, E., Santos-Victor, J., 2005. Least-square 3D reconstruction from one or more views and geometric clues. Computer Vision and Image Understanding 99 (2), 151-174.

Gruen, A., Zhang, L., 2005. Sensor modeling for aerial triangulation with Three-Line-Scanner (TLS) imagery. Journal of Photogrammetrie, Fernerkundung, Geoinformation (PFG) 2005 (2), 85-98.

Heikkinen, J., 2004. Accuracy analysis of circular image block adjustment. Proceedings of the International Archives

of the Photogrammetry, Remote Sensing and Spatial Information Sciences 35 (Part B5) 30-36.

Hernández, C., Schmitt, F., Cipolla, R., 2007. Silhouette coherence for camera calibration under circular motion. IEEE Transactions on Pattern Analysis and Machine Intelligence 29 (2), 343-349.

Hrabácek, J., van den Heuvel, F. A., 2000. Weighted geometric objects constraints integrated in a line-photogrammetric bundle adjustment. Proceedings of the International Archives of the Photogrammetry, Remote Sensing and Spatial Information Sciences 32 (Part B5), 380-387.

Jacobsen, K., 1999. Combined bundle block adjustment with attitude data. Proceedings of ASPRS Annual Convention, Portland, Oregon, (on CD-ROM).

Lichti, D. D., Kim, C., Jamtsho, S., 2010. An integrated bundle adjustment approach to range camera geometric self-calibration. ISPRS Journal of Photogrammetry and Remote Sensing 65 (4), 360-368.

Malm, H., Heyden, A., 2001. Stereo head calibration from a planar object. Proceedings of the 2001 IEEE Computer Society Conference on Computer Vision and Pattern Recognition 2, 657-662.

Mass, H. G., 2009. Image sequence based automatic multi-camera system calibration techniques. ISPRS Journal of Photogrammetry and Remote Sensing 29 (5-6), 352-359.

Mikhail, E. M., Bethel, J. S., McGlone, J. C., 2001. Introduction to Modern Photogrammetry. John Wiley & Sons Inc., New York, NY.

Nistér, D., 2004. An efficient solution to the five-point relative pose problem. IEEE Transactions on Pattern Analysis and Machine Intelligence 26 (6), 756-777.

Remondino, F., Fraser, C., 2006. Digital camera calibration methods: considerations and comparisons. Proceedings of the International Archives of the Photogrammetry, Remote Sensing and Spatial Information Sciences 36 (Part B5), 266-272.

Stewénius, H., Engels, C., Nistér, D., 2006. Recent developments on direct relative orientation. ISPRS Journal of Photogrammetry and Remote Sensing 60 (4), 284-294.

Triggs, B., McLauchlan, P., Hartley, R., Fitzgibbon, A., 2000. Bundle adjustment – a modern synthesis. In: Vision Algorithms: Theory and Practice, pp. 298-375.

van den Heuvel, F. A., 1998. 3D reconstruction from a single image using geometric constraints. ISPRS Journal of Photogrammetry and Remote Sensing 53 (6), 354-368.

Zhang, H. W., Zhang, Z. X., Zhang, J. Q., 2005. Analysis for the redundancy and relativity of the observation in generalized point photogrammetry. Proceedings of the International Symposium on Multispectral Image Processing and Pattern Recognition, Wuhan, China, 6045 (2), 1-8.

Zhang, Y. J., Zhang, Z. X., Sun, M. W., Ke, T., 2011. Precise orthoimage generation of Dunhuang wall painting. Photogrammetric Engineering and Remote Sensing 77 (6), 631-640.

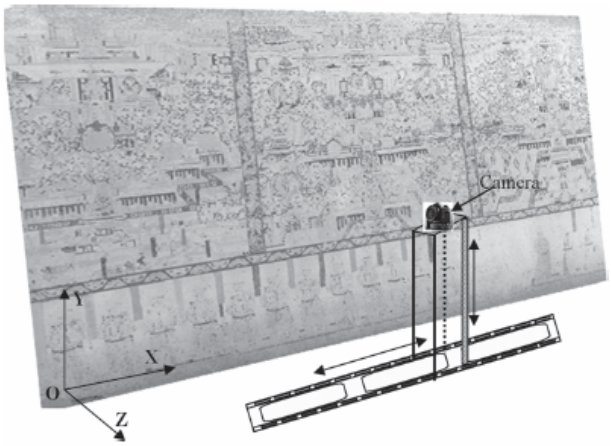

Fig. 1 Photographic structure of the painting (Zhang et al., 2011)

Table 1 Correlation coefficient of exterior orientation parameters

Item	Xs			Ys			Zs		
	Max	Min	Mean	Max	Min	Mean	Max	Min	Mean
φ	0.9998	0.9954	0.9990	0.0067	0.0000	0.0010	0.7522	0.0000	0.1346
ω	0.0272	0.0000	0.0034	0.9997	0.9984	0.9991	0.6180	0.0090	0.4167
κ	0.3057	0.0001	0.0422	0.6014	0.0002	0.0707	0.2572	0.0001	0.0293

Table 2 Theoretical accuracy of unknowns in Model I and Model II (without control points)

Item	Model I			Model II		
	Max	Min	Mean	Max	Min	Mean
Xs(mm)	0.12032	0.02315	0.05673	0.10810	0.01850	0.05252
Ys(mm)	0.15132	0.03526	0.08427	0.09570	0.02663	0.05062
Zs(mm)	0.30727	0.06721	0.13930	0.04026	0.00556	0.02412
$\varphi_{(rad)}$	0.00162	0.00042	0.00074	0.00109	0.00029	0.00037
$\omega_{(rad)}$	0.00164	0.00065	0.00112	0.00108	0.00040	0.00052
$\kappa_{(rad)}$	0.00049	0.00011	0.00021	0.00039	0.00010	0.00019
X(mm)	1.12597	0.00227	0.04846	0.11803	0.00269	0.04781
Y(mm)	1.32630	0.00257	0.04469	0.08769	0.00308	0.04003
Z(mm)	4.81030	0.01159	0.13717	0.08758	0.01397	0.03390

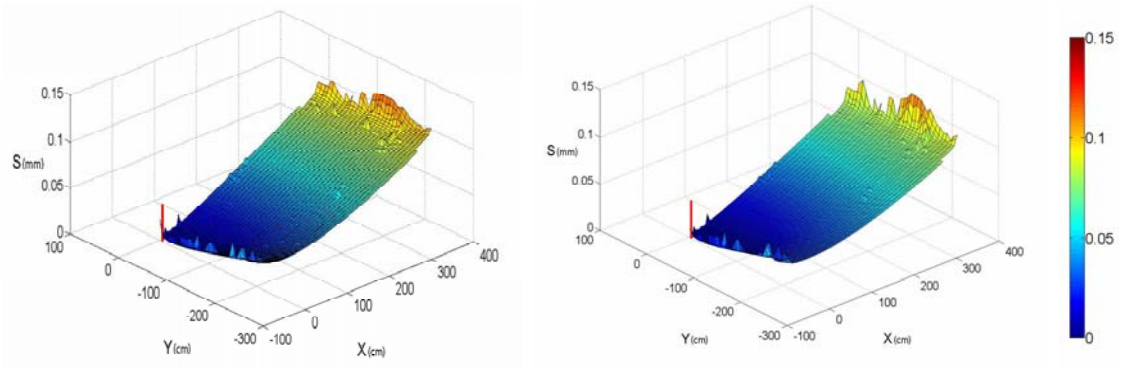

(a) RMS error of X (Model I) (b) RMS error of X (Model II)

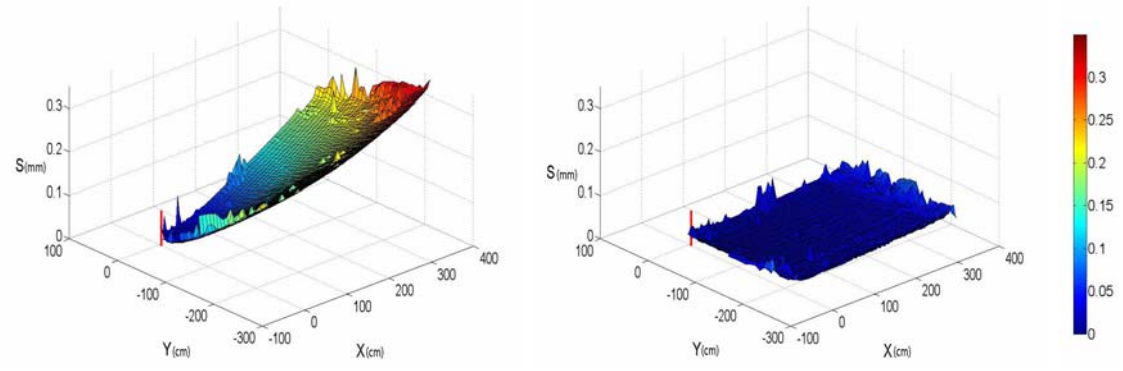

(c) RMS error of Z (Model I) (d) RMS error of Z (Model II)

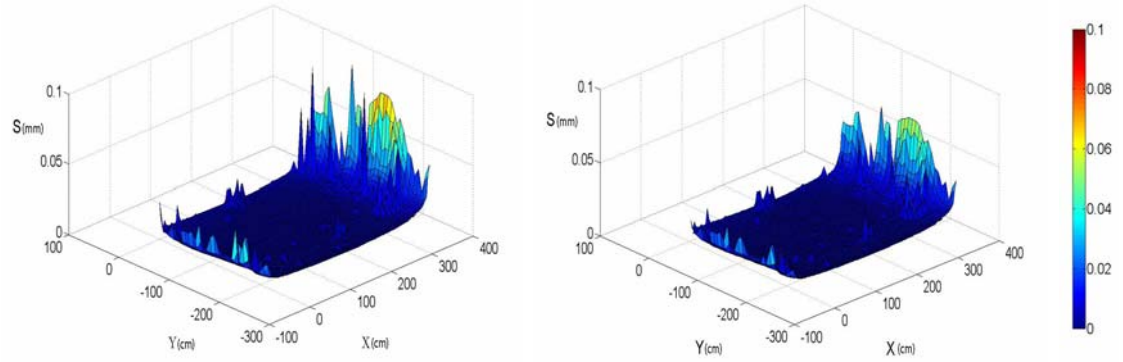

(e) RMS error of X (Model III) (f) RMS error of X (Model IV)

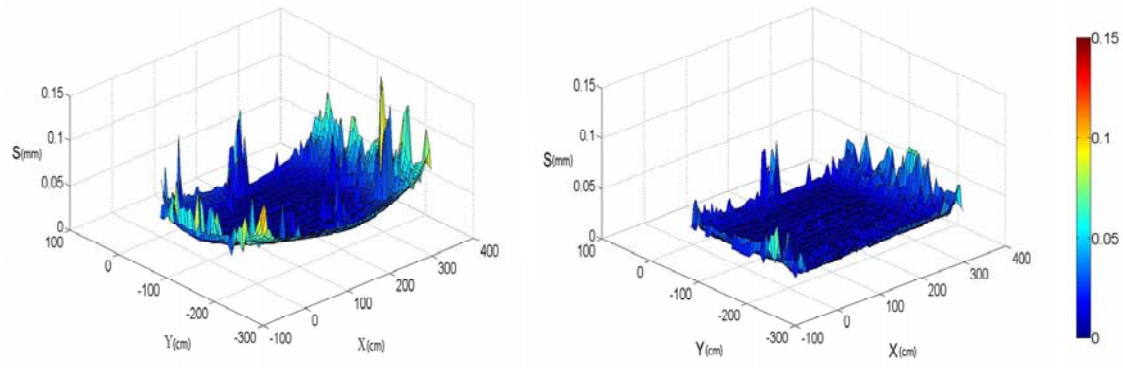

(g) RMS error of Z (Model III) (h) RMS error of Z (Model IV)

Fig. 2. Theoretical accuracy distribution of object points: (a) and (b), (c) and (d) are the RMS errors of Model I and Model II in the X and Z direction, respectively; (e) and (f), (g) and (h) are the RMS errors of Model III and Model IV in the X and Z direction, respectively.

Table 3 Theoretical accuracy of unknowns in Model III and Model IV (with control points)

Item	Model III			Model IV		
	Max	Min	Mean	Max	Min	Mean
Xs(mm)	0.08468	0.01607	0.02524	0.04890	0.01524	0.02093
Ys(mm)	0.08869	0.02249	0.03691	0.05340	0.02026	0.02825
Zs(mm)	0.05368	0.00889	0.01718	0.01924	0.00726	0.01023
φ (rad)	0.00151	0.00026	0.00042	0.00086	0.00025	0.00032
ω (rad)	0.00141	0.00039	0.00061	0.00085	0.00035	0.00045
κ (rad)	0.00041	0.00005	0.00011	0.00030	0.00005	0.00008
X(mm)	0.37405	0.00305	0.00696	0.06051	0.00322	0.00648
Y(mm)	0.41406	0.00304	0.00676	0.04232	0.00321	0.00625
Z(mm)	1.24470	0.00592	0.02906	0.06472	0.00610	0.02143

Table 4 Actual accuracy of check points in Model III and Model IV (with control points).

Item	Model III			Model IV		
	RMS	Mean	Max/Min	RMS	Mean	Max/Min
X(mm)	0.34848	0.04626	-1.04525	0.33093	0.02621	-0.94774
Y(mm)	0.35017	0.03852	1.58983	0.32510	0.01870	1.48296
Z(mm)	0.79274	0.39363	1.91129	0.47234	0.14471	-1.10434

Table 5 Solutions under different weights of constraints (without control points)

Item	Weight I	Weight II	Unit weight RMS error	Condition number	Iteration times	Mean X (mm)	Mean Y (mm)	Mean Z (mm)
Test I	1.0	0.0001	0.006861	2.8977*10^24	7	0.04917	0.04274	0.06124
Test II		0.001	0.007511	2.8386*10^24	6	0.04819	0.04014	0.06004
Test III		0.01	0.008501	2.5300*10^26	6	0.05008	0.04350	0.06457
Test IV	10.0	0.0001	0.006882	2.6975*10^24	9	0.04897	0.04110	0.03509
Test V		0.001	0.007504	2.0692*10^24	7	0.04795	0.04011	0.03430
Test VI		0.01	0.008656	1.7963*10^26	7	0.04949	0.04301	0.03459
Test VII	100.0	0.0001	0.006983	1.8819*10^24	21	0.04395	0.03875	0.02740
Test VIII		0.001	0.007544	1.7618*10^24	11	0.04380	0.03749	0.02716
Test IX		0.01	0.008676	1.5151*10^26	15	0.04801	0.04026	0.02897